Eur. Phys. J. A **5**, 307–319 (1999)

THE EUROPEAN PHYSICAL JOURNAL A

Subthreshold and near threshold K^+ meson production on light nuclei by protons

E.Ya. Paryev

Institute for Nuclear Research, Russian Academy of Sciences, 117312 Moscow, Russia

Received: 26 October 1998 / Revised version: 10 February 1999
Communicated by W. Weise

Abstract. The inclusive K^+ meson production in proton–nucleus collisions in the near threshold and subthreshold energy regimes is analyzed with respect to the one–step ($pN \to K^+YN, Y = \Lambda, \Sigma$) and two–step ($pN \to NN\pi, NN2\pi$; $\pi N \to K^+Y$) incoherent production processes on the basis of an appropriate folding model, which takes properly into account the struck target nucleon removal energy and momentum distribution (nucleon spectral function), novel elementary cross sections for proton–nucleon reaction channel close to threshold as well as nuclear mean–field potential effects on the one–step and two–step kaon creation processes. A detailed comparison of the model calculations of the K^+ total and differential cross sections for the reactions $p + Be^9$ and $p + C^{12}$ with the existing experimental data is given, illustrating both the relative role of the primary and secondary production channels at considered incident energies and those features of the cross sections which are sensitive to the high momentum and high removal energy part of the nucleon spectral function. It is found that, contrary to previous studies performed in the literature, the pion–nucleon production channels do not necessarily dominate in pA collisions at subthreshold energies and the relative strength of the proton and pion induced reaction channels in light target nuclei in the subthreshold energy regime is governed by the kinematics of experiment under consideration.

PACS. 25.40.-h Nucleon-induced reactions

1 Introduction

Kaon production in proton–nucleus reactions at bombarding energies less than threshold energies in a collision of free nucleons has been extensively studied both experimentally and theoretically in recent years [1–12]. Since kaons have a long mean free path inside the nucleus, it is expected to extract from these studies valuable information about the nuclear structure at short nucleon–nucleon separations as well as about the dynamics of the reaction, properties of the produced particles in the nuclear environment. The first theoretical investigations of subthreshold kaon production on nuclei have been performed in the framework of the respective folding models based on both the direct mechanism [1, 2, 6, 11, 12] of K^+ production ($pN \to K^+\Lambda N$) and on the two–step mechanism [1, 3–5] associated with the production of kaons by intermediate pions ($pN_1 \to \pi NN$, $\pi N_2 \to K^+\Lambda$) using different parametrizations for the elementary kaon production cross sections as well as for the internal nucleon momentum distribution. In these folding models only the nucleon momentum distribution has been used and the off–shell propagation of the struck target nucleon has been neglected or has been taken into account the most crudely, but it could be significant in the threshold heavy meson production processes, since they are limited by the phase space. Later [8–10] the full nucleon momentum and binding (removal) energy distribution (nucleon spectral function) has been properly taken into account in calculating the subthreshold kaon production in pC and pPb collisions. It has been shown that within the spectral function approach the measured total [1] and differential [8] K^+ production cross sections are underestimated significantly at subthreshold incident energies by calculations assuming only first chance collisions unaffected [8, 10] by the nuclear medium or affected [9] by the repulsive impinging proton optical potential. When the two–step kaon production processes with intermediate pions have been taken into consideration, the results of calculations [8, 9] are in much better agreement with the experimental data, while the ones from [10] have shown that without the in–medium modifications of the available for pion and kaon production invariant energies due to the corresponding optical potentials it is not possible to reproduce at subthreshold energies via the secondary pion induced channels the considered experimental data on total [1] and differential [8] K^+ cross sections from pC interactions. However, in order to gain a deeper insight into the relative role of the primary and secondary reaction channels, it is obviously necessary, as was pointed out in [10], to carry out a detailed study of subthreshold kaon production in pA collisions on the basis of the spectral function approach that

includes consistently the mean–field potential effects both on the one–step and on two–step kaon production processes. This is the main purpose of the present article. In doing so, it is extremely important to incorporate in the calculations new experimental data points for the total cross section of the $pp \to K^+\Lambda p$ reaction in the threshold region covering the excess energy range up to 7 MeV from the COSY–11 collaboration at COSY–Jülich [13], which lie above the current parametrizations [10, 14, 15] employed in the recent studies of the subthreshold kaon production in proton–nucleus [10] and heavy–ion [14, 15] reactions as well as to analyze another experimental data on subthreshold and near threshold K^+ production in pA interactions obtained at the ITEP proton synchrotron [11, 12] together with those presented in [1, 8].

In the present work we have performed an analysis of the K^+ production from pBe and pC reactions in the near threshold and subthreshold energy regimes using the spectral function approach [10] that has been modified to take into account the new data points for $pp \to K^+\Lambda p$ reaction close to threshold [13] as well as to treat the mean–field potential effects on the primary and secondary creation processes on an equal footing. This approach is explained in detail in [10], here we only describe the respective modifications.

2 The model and inputs

2.1 Direct K^+ production processes

Apart from participation in the elastic scattering an incident proton can produce a K^+ directly in the first inelastic pN collision due to nucleon Fermi motion. Since we are interested in a few GeV region (up to 3 GeV), we have taken into account [16] the following elementary processes which have the lowest free production thresholds:

$$p + N \to K^+ + \Lambda + N, \tag{1}$$

$$p + N \to K^+ + \Sigma + N. \tag{2}$$

Following the predictions of the effective chiral Lagrangian approach by Kaplan and Nelson [17], we assume that the mass of the produced kaon is not changed in the nuclear medium (see, also, [14, 15, 18]) due to an approximate cancellation of attractive scalar and repulsive vector mean fields[1], i.e., the total energy E_{K^+} of the K^+ meson with momentum $\mathbf{p}_{K^+}$ is given by:

$$E_{K^+} = \sqrt{\mathbf{p}_{K^+}^2 + m_K^2}, \tag{3}$$

where m_K is the rest mass of a kaon in free space. The effective masses m_h^* of other final hadrons (nucleon and hyperon) participating in the K^+ production processes (1), (2), which have to be incorporated in our model [10] (see below) instead of their free space masses m_h to allow for the influence of the nuclear environment on the K^+ production, are defined by the following dispersion relation [27–33]:

$$E_h^2 = \mathbf{p}_h^2 + m_h^{*2} = (\sqrt{\mathbf{p}_h^2 + (m_h + U_s^h)^2} + U_v^h)^2, \tag{4}$$

where U_s^h and U_v^h are the scalar and vector (time–like component) self–energies of hadron h, $\mathbf{p}_h$ denotes its canonical three–momentum[2]. Use the relativistic dispersion relation for the quasiparticle given by the l.h.s. of (4) enables us to keep on dealing with relativistic kinematics as in the on–mass shell case. The effective masses m_h^* include the effective scalar mean–field potentials U_{eff}^h, needed for our calculations:

$$m_h^* = m_h + U_{eff}^h. \tag{5}$$

Equations (4) and (5) allow to extract these potentials provided that the scalar and vector fields U_s^h and U_v^h are known. In the general case these fields are density– and momentum–dependent [27, 31–33]. However, for the purposes of the present study as well as for reasons of simplicity it is sufficient to neglect the explicit momentum dependence of U_s^h and U_v^h and to evaluate the effective fields U_{eff}^h knowing the quantities U_s^h and U_v^h only in a very limited density and momentum range relevant for the observed [1, 8, 11, 12] subthreshold kaon production in pA reactions. Since the K^+ creation due to first–chance pN collisions (1), (2) occurs mainly inside the target nucleus [34] and populates as showed our calculations the outgoing nucleon and hyperon in a limited kinematical range with the average kinetic energies ≤ 0.1 GeV for the most part of kinematical conditions of the experiments on subthreshold kaon production which will be analyzed below, the potentials U_s^h and U_v^h should be estimated at the normal nuclear matter density for the above characteristic energy. Employing the recent parametrization for the nucleon scalar and vector potentials from [33], obtained within the self–consistent Dirac–Brueckner approach, it can readily be found that the nucleon effective potential U_{eff}^N at kinetic energy of 100 MeV for normal matter density becomes $U_{eff}^N = -34$ MeV. It may be pointed out that this value of the effective potential U_{eff}^N is in good agreement [10] with the characteristic depth of a potential well gained in the noninteracting Fermi–gas model.

At present there are a few models for the hyperon mean–field potentials in nuclear medium [35–37], which give essentially different predictions for the actual magnitude of the potentials. Thus, for example, in the naive constituent quark model the hyperon self–energies are about $\frac{2}{3}$ of the nucleon self–energies. This assumption is widely used in the relativistic transport models for high–energy nucleus–nucleus collisions [15, 32, 37–39]. In view

[1] It should be remarked that the actual magnitude of these fields is still a matter of current debate [19–25], although recent studies [15, 26] indicate that a weakly repulsive kaon potential (≈ 30 MeV at the normal nuclear matter density) cannot be excluded by the present data on kaon transverse flow in heavy–ion collisions, measured by the FOPI Collaboration at SIS/GSI.

[2] The space–like components of the vector self–energies are ignored here [33].

of the substantial uncertainties of the model hyperon self–energies as well as since at subthreshold energies hyperons from primary pN interactions (1) and (2) are produced, as was noted above, in a limited kinematical range, it is naturally to use for the effective potentials U^{Λ}_{eff} and U^{Σ}_{eff} seen by the final low–energy Λ and Σ hyperons the values of the corresponding optical potentials at normal nuclear matter density, extracted from the properties of hypernuclei, namely: $U^{\Lambda}_{eff} = -30\ MeV$ [37, 40, 41] and $U^{\Sigma}_{eff} = -26\ MeV$ [41]. The set of parameters:

$$\begin{aligned} U^{N}_{eff} &= -34\ MeV, \\ U^{\Lambda}_{eff} &= -30\ MeV, \\ U^{\Sigma}_{eff} &= -26\ MeV \end{aligned} \tag{6}$$

we will use throughout our calculations. To see the sensitivity of kaon production cross section from the one–step processes (1), (2) to the effective nucleon and hyperon potentials, we will also ignore these potentials in our calculations as this has been done in the previous investigations [8–10] of subthreshold K^+ production in pA collisions within the spectral function approach.

Another medium effect that must be taken yet into account is the modification of the four–momentum $\hat{p}_0 = (E_0, \mathbf{p}_0)$ ($\hat{p}_0^2 = m_N^2$) of incoming proton inside the target nucleus due to the nuclear optical potential V_0. Let $\hat{p}_0^{'} = (E_0^{'}, \mathbf{p}_0^{'})$ be the four–momentum of incident proton under the influence of this potential, whereas $\hat{p}_A = (M_A, 0)$ and $\hat{p}_A^{'} = (M_A + \frac{\Delta\mathbf{p}^2}{2M_A}, \Delta\mathbf{p})$ be the four–momenta of the initial with mass M_A and recoiling (due to the refraction of a beam proton at the nuclear surface) with momentum $\Delta\mathbf{p}$ target nucleus, respectively. Energy and momentum conservation reads:

$$\hat{p}_0 + \hat{p}_A = \hat{p}_0^{'} + \hat{p}_A^{'}. \tag{7}$$

This leads to the following expressions for the total energy $E_0^{'}$ and momentum $\mathbf{p}_0^{'}$ of the incident proton inside the target nucleus:

$$E_0^{'} = E_0 - \frac{\Delta\mathbf{p}^2}{2M_A}, \tag{8}$$

$$\mathbf{p}_0^{'} = \mathbf{p}_0 - \Delta\mathbf{p}. \tag{9}$$

Taking into consideration that, on the other hand,

$$E_0^{'} = \sqrt{(\mathbf{p}_0 - \Delta\mathbf{p})^2 + m_N^2} + V_0 \tag{10}$$

and assuming for the sake of numerical simplicity that the recoil momentum $\Delta\mathbf{p}$ of the target nucleus entering in the (8) and (9) is parallel to the beam direction

$$\Delta\mathbf{p} = \Delta p \frac{\mathbf{p}_0}{|\mathbf{p}_0|}, \tag{11}$$

we can readily get the following expression for the quantity Δp:

$$\begin{aligned} \Delta p &= \frac{p_0 E_0^2 M_A \left(1 - \sqrt{1 - \frac{2V_0 E_0^2}{p_0^2 M_A} - \frac{2V_0 m_N^2}{p_0^2 E_0}}\right)}{(E_0^3 + m_N^2 M_A)} \\ &\approx \frac{E_0}{p_0} V_0, \end{aligned} \tag{12}$$

where $p_0 = |\mathbf{p}_0|$. According to [3, 5, 32, 33, 42], a proton impinging on a nucleus at the kinetic energy ϵ_0 of about $\epsilon_0 \approx 1\ GeV$ feels in the interior of the nucleus the repulsive optical potential of about $V_0 \approx 40\ MeV$. We will use this value of potential V_0 also at higher beam energies considered in the present work. Then, in the energy range under consideration, i.e., when the energy ϵ_0 varies within the range of about 1–3 GeV the "recoil momentum" Δp as it follows from (12) amounts approximately to 43 MeV/c.

Further, let E_t and $\mathbf{p}_t$ be the total energy and momentum of the struck target nucleon N just before the collisions (1), (2). Taking into account the respective recoil and excitation energies of the residual $(A-1)$ system, one has [10, 43, 44]:

$$E_t = M_A - \sqrt{(-\mathbf{p}_t)^2 + (M_A - m_N + E)^2}, \tag{13}$$

where E is the removal energy of the struck target nucleon. It is easily seen that in this case the struck target nucleon is off–shell. After specifying the energies and momenta all particles involved in the K^+ production processes (1), (2) we can write out the corresponding energy and momentum conservation:

$$E_0^{'} + E_t = E_{K^+} + E_Y + E_N, \tag{14}$$

$$\mathbf{p}_0^{'} + \mathbf{p}_t = \mathbf{p}_{K^+} + \mathbf{p}_Y + \mathbf{p}_N. \tag{15}$$

From (14) and (15) we obtain the squared invariant energy available in the first chance pN collision:

$$s = (E_0^{'} + E_t)^2 - (\mathbf{p}_0^{'} + \mathbf{p}_t)^2. \tag{16}$$

On the other hand, according to the (14), (15), one gets:

$$s = (E_{K^+} + E_Y + E_N)^2 - (\mathbf{p}_{K^+} + \mathbf{p}_Y + \mathbf{p}_N)^2. \tag{17}$$

Using (3)–(5), this leads to the following expression for the in–medium reaction thresholds:

$$\sqrt{s^*_{th}} = m_K + m_Y^* + m_N^* = \sqrt{s_{th}} + U^Y_{eff} + U^N_{eff}, \tag{18}$$

where $\sqrt{s_{th}} = m_K + m_Y + m_N$ are the threshold energies in free space and the effective potentials are given by (6). Hence, the reduction of the K^+ threshold in the medium will be 64 MeV in the case of $pN \to K^+\Lambda N$ reaction and 60 MeV for the $pN \to K^+\Sigma N$ process. This will strongly enhance the K^+ production via first chance pN collisions (see, below).

Finally, neglecting the kaon final–state interactions [10], we can describe the invariant inclusive cross section of K^+ production on nuclei from the primary proton induced reaction channels (1) and (2) by the formulas (3)–(6) from [10]. The invariant inclusive cross sections for K^+ production in the elementary processes (1), (2) appearing in (6)

Table 1. Parameters in the approximation of the partial cross sections for the production of K^+ mesons in pp–collisions

Reaction	A_Y,$\mu b \cdot GeV^{-2}$	B_Y, GeV^{-2}	C_Y,$\mu b \cdot GeV^{-2}$	s_{th},GeV^2
$p+p \to K^+ + \Lambda + p$	122.943	2.015	2515.56	6.490
$p+p \to K^+ + \Sigma + N$	104.026	1.006	0.	6.880

[10] have been described in the present work also by the three–body phase space calculations (formulas (9)–(12) from [10] in which one has to make the following substitutions: $m_N \to m_N^*$, $m_Y \to m_Y^*$, $E_0 \to E_0^{'}$, $\mathbf{p}_0 \to \mathbf{p}_0^{'}$) normalized to the corresponding "in–medium" total cross sections $\sigma_{pN\to K^+YN}(\sqrt{s}, \sqrt{s_{th}^*})$. The "in-medium" cross sections $\sigma_{pN\to K^+YN}(\sqrt{s}, \sqrt{s_{th}^*})$ are equivalent [14, 15] to the vacuum cross sections $\sigma_{pN\to K^+YN}(\sqrt{s}, \sqrt{s_{th}})$ in which the free thresholds $\sqrt{s_{th}}$ are replaced by the effective thresholds $\sqrt{s_{th}^*}$ as given by (18). For the free total cross sections $\sigma_{pN\to K^+YN}(\sqrt{s}, \sqrt{s_{th}})$ we have used the parametrization suggested in [10] that has been corrected for the new data points for $pp \to K^+\Lambda p$ reaction from the COSY–11 collaboration at COSY–Jülich [13] in the threshold region covering the excess energy range up to 7 MeV, viz.:

$$\sigma_{pp\to K^+YN}(\sqrt{s}, \sqrt{s_{th}}) = \frac{A_Y(s-s_{th})^2}{4m_p^2 + B_Y(s-s_{th})^2} \qquad (19)$$
$$+C_Y(s-s_{th})^2[0.5-(s-s_{th})/GeV^2]^{2.328}$$
$$\times\Theta[0.5-(s-s_{th})/GeV^2]/(4m_p^2),$$

where $\Theta(x) = (x+|x|)/2|x|$ and the constants A_Y, B_Y, C_Y and s_{th} are given in Table 1. The comparison of the results of our calculations by (19) (solid line) with the experimental data close to the threshold for $pp \to K^+\Lambda p$ reaction from the installation COSY–11 [13] (full squares), from the facility TOF at COSY [13] (full dots) as well as from the old bubble chamber measurements [45] (open crosses) is shown in Figure 1. It is seen that our parametrization (19) fits quite well the world set of data for the $pp \to K^+\Lambda p$ reaction in the threshold region.

The effective numbers of nucleons for the $pN \to K^+YN$ reaction on Be^9 and C^{12} target nuclei have been calculated in the case of Gaussian nuclear density ($\rho(\mathbf{r}) = (b/\pi)^{3/2}\exp(-br^2)$, $b = 0.240$ fm^{-2} for Be^9 and $b = 0.248$ fm^{-2} for C^{12}) in accordance with the formula (17) from [10].

Another a very important ingredient for the calculation of the K^+ production cross sections in proton–nucleus reactions in the subthreshold energy regime– the nucleon spectral function $P(\mathbf{p}_t, E)$ (which represents the probability to find in the nucleus a nucleon with momentum $\mathbf{p}_t$ and removal energy E) for C^{12} target nucleus was taken from [10] (see, also, [46–52]). For K^+ production calculations in the case of Be^9 target nucleus reported here we have employed for the single–particle (uncorrelated) part $P_0(\mathbf{p}_t, E)$ of the nucleon spectral function the same expression as that used for C^{12} target nucleus, but in which the s– and p–shell binding energies $|\epsilon_{1s}|$ and $|\epsilon_{1p}|$ were taken from [53, 54]: $|\epsilon_{1s}| = 26$ MeV, $|\epsilon_{1p}| = 16$ MeV as well as the parameter b_0 determining the s– and p–shell

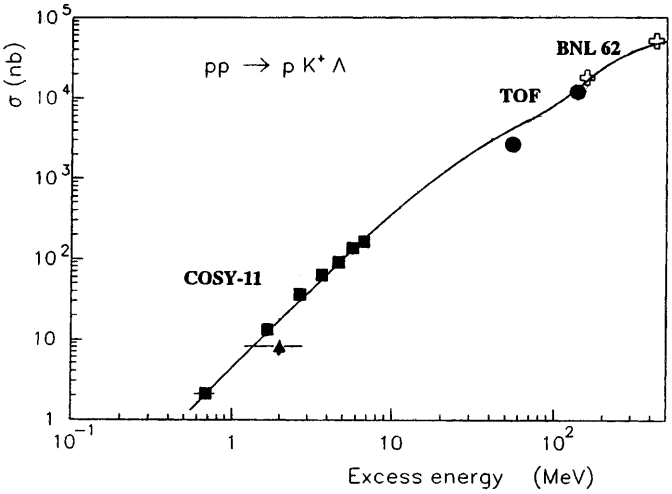

Fig. 1. The total cross section for $pp \to K^+\Lambda p$ reaction as a function of an excess energy ($\sqrt{s} - \sqrt{s_{th}}$). For notation see text

nucleon momentum distributions $n_{1s}(\mathbf{p}_t)$ and $n_{1p}(\mathbf{p}_t)$ was set to 77.5 (GeV/c)$^{-2}$. In our calculations of the K^+ production cross sections on Be^9 the high momentum and high removal energy part (correlated part) $P_1(\mathbf{p}_t, E)$ of the nucleon spectral function has been used in the simple analytical form given in [10], in which the two–particle break–up threshold E_{thr} was taken to be 19 MeV and the other parameters appearing in the $P_1(\mathbf{p}_t, E)$ were identical to those for C^{12}.

Let us consider now the two–step K^+ production mechanism.

2.2 Two–step K^+ production processes

Kinematical considerations show that in the bombarding energy range of our interest (≤ 3.0 GeV) the following two–step production processes may not only contribute to the K^+ production in pA interactions but even dominate [1, 3–5, 8–10] at subthreshold energies. An incident proton can produce in the first inelastic collision with an intranuclear nucleon also a pion through the elementary reactions:

$$p + N_1 \to N + N + \pi, \qquad (20)$$

$$p + N_1 \to N + N + 2\pi. \qquad (21)$$

We remind that the free threshold energies for these reactions are, respectively, 0.29 and 0.60 GeV. Then the intermediate pion, which is assumed to be on–shell, produces the kaon on a nucleon of the target nucleus via the

elementary subprocesses with the lowest free production thresholds (respectively, 0.76 and 0.89 GeV):

$$\pi + N_2 \to K^+ + \Lambda, \tag{22}$$

$$\pi + N_2 \to K^+ + \Sigma, \tag{23}$$

provided that these subprocesses are energetically possible. Since the main contribution to the K^+ production at subthreshold incident energies comes from a very fast pions moving in the beam direction, the relevant kinetic energy ϵ_N of each nucleon produced in the reactions (20), (21) together with a high–energy pion can be approximately estimated as $\epsilon_N \approx 0.1\ GeV$ [10] at beam energies of our interest. As has been mentioned above (see, (6)), such low–energy outgoing nucleons feel inside the nucleus the attractive effective potential $U^N_{eff} = -34\ MeV$ that reduces their free masses in line with the formula (5). Thus, it is necessary to incorporate properly the effective nucleon mass m^*_N in calculations of the K^+ production cross section from the two–step processes (20)–(23). Moreover, it should be taken into account in these calculations also the same in–medium modification of the masses of hyperons from secondary πN collisions (22) and (23) as that for hyperons from primary pN collisions due to the corresponding effective potentials U^{Λ}_{eff} and U^{Σ}_{eff} (see, (5), (6)). Keeping in mind this fact, we can represent the K^+ production cross section for pA reactions from the secondary pion induced reaction channels (22) and (23) by the expressions like the formulas (52)–(100) from [10]. As compared with [10], the equations describing the inclusive invariant differential cross sections $E_\pi d\sigma_{pN\to\pi X}/d\mathbf{p}_\pi$ for pion production in the elementary reactions (20), (21) and the maximum momentum p^{max}_π of a pion created in these reactions include the effective mass m^*_N of the secondary nucleons instead of their free mass m_N as well as the in–medium four–momentum $\hat{p}^{'}_0 = (E^{'}_0, \mathbf{p}^{'}_0)$ of incident proton instead of its initial four–momentum $\hat{p}_0 = (E_0, \mathbf{p}_0)$. And the expressions describing the Lorentz invariant inclusive cross sections for K^+ production in πN collisions via the subprocesses (22), (23) include now the effective hyperon mass m^*_Y instead of its rest mass m_Y in free space. For the total cross sections $\sigma_{pN\to NN\pi}$, $\sigma_{pN\to NN2\pi}$ and $\sigma_{\pi N\to K^+Y}$ of the elementary processes (20), (21) and (22), (23) we have used in this study the same parametrizations as those employed in [10] (see, also, [55–57]), but in which the corresponding threshold energies have been properly corrected for the effective mass m^*_N of the secondary nucleons and for the effective hyperon mass m^*_Y, respectively. It is interesting to note that both the parametrization (81) from [10] for the total cross section $\sigma_{\pi^+n\to K^+\Lambda}$ of reaction $\pi^+n \to K^+\Lambda$ and those from [18, 58] lead to similar results for the respective kaon production cross sections in pA collisions at subthreshold incident energies. Thus, the medium effects under consideration have been taken into account in calculating kaon production cross section from the secondary pion induced reaction channels (22) and (23) on the same covariant footing[3] as that employed in calculation the K^+ production cross section from primary proton induced reaction channels (1) and (2). Results of investigations [10] indicate that the main contribution to the K^+ production in the two–step reaction channels (20)–(23) both at subthreshold and above the free NN threshold incident energies comes from the use only of the uncorrelated part $P_0(\mathbf{p}_t, E)$ of the nucleon spectral function. Therefore, we will adopt hereafter only the $E_{K^+}\frac{d\sigma^{(sec)}_{00}(\mathbf{p}_0)}{d\mathbf{p}_{K^+}}$ term in the sum (52) [10] to calculate the K^+ yield in pA interactions from the secondary channels (22) and (23).

To show the validity of the present approach in the description of the kaon yield in pA collisions from these channels, it is obviously necessary to be able to reproduce within this approach the high momentum parts of the charged pion spectra measured at forward laboratory angles at beam energies between 1 and 2 GeV. Taking into consideration the pion final–state absorption, we easily get the following expression for the invariant inclusive cross section of pion production on nuclei from the primary proton induced reaction channels (20) and (21) (see, also, [16]):

$$E_\pi \frac{d\sigma^{(prim)}_{pA\to\pi X}(\mathbf{p}_0)}{d\mathbf{p}_\pi} = I^{'}_V[A]\left\langle E_\pi \frac{d\sigma_{pN\to\pi X}(\mathbf{p}_0, \mathbf{p}_\pi)}{d\mathbf{p}_\pi}\right\rangle, \tag{24}$$

where

$$I^{'}_V[A] = A\int \rho(\mathbf{r})d\mathbf{r}\exp[-\mu(p_0)\int\limits_{-\infty}^{0}\rho(\mathbf{r}+x\mathbf{\Omega}_0)dx - \mu(p_\pi) \times \int\limits_0^{\infty}\rho(\mathbf{r}+x\mathbf{\Omega}_\pi)dx], \tag{25}$$

$$\left\langle E_\pi \frac{d\sigma_{pN\to\pi X}(\mathbf{p}_0, \mathbf{p}_\pi)}{d\mathbf{p}_\pi}\right\rangle = \int\!\!\int P(\mathbf{p}_t, E)d\mathbf{p}_t dE \times \left[E_\pi \frac{d\sigma_{pN\to\pi X}(\sqrt{s}, \mathbf{p}_\pi)}{d\mathbf{p}_\pi}\right], \tag{26}$$

$$\mu(p_0) = \sigma^{in}_{pp}(p_0)Z + \sigma^{in}_{pn}(p_0)N,$$
$$\mu(p_\pi) = (A/2)[\sigma^{tot}_{\pi p}(p_\pi) + \sigma^{tot}_{\pi n}(p_\pi)]. \tag{27}$$

Here, $\sigma^{in}_{pN}(p_0)$ and $\sigma^{tot}_{\pi N}(p_\pi)$ are the inelastic and total cross sections of the free pN and πN interactions, respectively; $\mathbf{p}_\pi$ and E_π are the momentum and total energy of a pion, $\mathbf{\Omega}_\pi = \mathbf{p}_\pi/p_\pi$; Z and N are the numbers of protons and neutrons in the target nucleus (A=N+Z); $\mathbf{\Omega}_0 = \mathbf{p}_0/p_0$ ($\mathbf{p}_0$ is the beam momentum). As has been pointed out already above, the differential cross sections for pion production in pN collisions entering into the (26) take into account the medium effects under consideration. Since we are interested in the spectra of emitted pions at forward

[3] It should be noted that in [10] the nuclear mean–field effects on the kaon production cross section from pion induced reaction channels have been treated in a noncovariant manner. However, both treatments–present and that given in [10], as showed our calculations, lead to the close results.

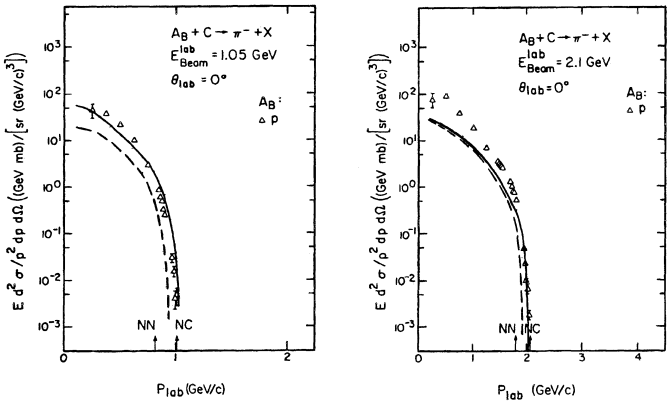

Fig. 2. Lorentz invariant negative pion inclusive cross sections versus the (lab) momentum at 0^0 for 1.05 (left) and 2.1 GeV (right) protons interacting with a carbon target. The experimental data (open triangles) are from [59]. The curves are calculation. The solid and dashed lines are our calculation by (24)–(28) for primary production processes (20), (21) with the total nucleon spectral function at $V_0 = 40\ MeV$, $U^N_{eff} = -34\ MeV$ and $V_0 = 0$, $U^N_{eff} = 0$, respectively. The arrows indicate the kinematical limits for pion production from free nucleons as well as from nucleon–nucleus interactions

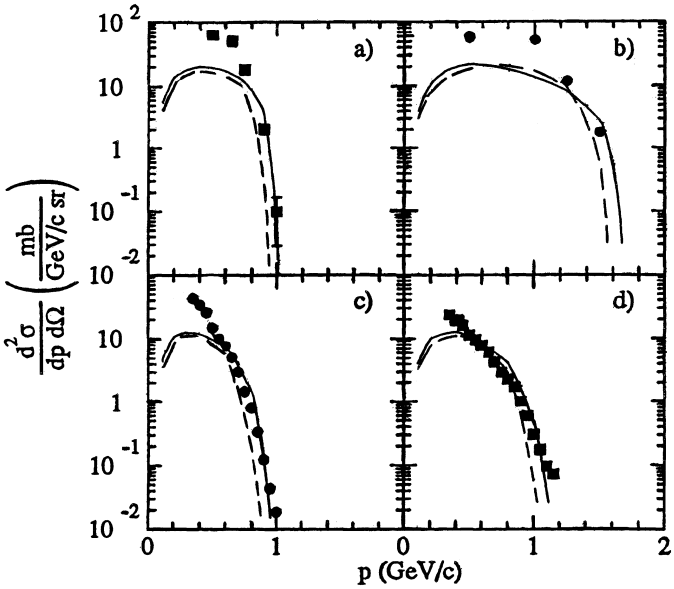

Fig. 3. Measured and calculated positive pion production cross sections in pC collisions at different bombarding energies and outgoing laboratory angles–a) 1.05 GeV, 0^0 [60]; b) 1.73 GeV, 0^0 [60]; c) 1.2 GeV, 40^0 [8]; d) 1.5 GeV, 40^0 [8]. The lines are results of our model at $V_0 = 40\ MeV$, $U^N_{eff} = -34\ MeV$–solid line, at $V_0 = 0$, $U^N_{eff} = 0$–dashed line

laboratory angles, i.e. when $\mathbf{\Omega}_\pi \approx \mathbf{\Omega}_0$, we can easily obtain in the case of a nucleus with the uniform density of nucleons of a radius $R = 1.3A^{1/3}$ fm the following simple form for the integral (25) [16]:

$$I^{'}_V[A] = \frac{3A}{(a_1 - a_2)a_2^2} \times\left\{1 - (1 + a_2)e^{-a_2} - (\frac{a_2}{a_1})^2[1 - (1 + a_1)e^{-a_1}]\right\}, \quad (28)$$

where $a_1 = 3\mu(p_\pi)/2\pi R^2$ and $a_2 = 3\mu(p_0)/2\pi R^2$. The comparison of the results of our calculations by (24)–(28) for the Lorentz invariant inclusive cross sections for the π^- meson production at 0^0 in the interaction of 1.05 and 2.1 GeV protons with C^{12} nuclei with the experimental data [59] is given in Fig. 2. The elementary cross sections σ^{in}_{pN} and $\sigma^{tot}_{\pi N}$ in the calculations were assumed to be, respectively, 30 and 35 mb [10]. One can see that our calculations reproduce quite well the high momentum tails of the pion spectra only if we include the effect of the mean fields (mainly the nucleon effective potential U^N_{eff}) on the one–step production processes (20), (21). Let us discuss now the results for π^+ meson production. In Fig. 3 we compare the results of our calculations by (24)–(28) for the double differential cross sections for π^+ production in pC collisions at different incident energies and outgoing angles with the experimental data [8, 60]. It is seen that the agreement between the model calculations and the measurements in the high momentum parts of the π^+ spectra is quite remarkable, as in the above comparison for the π^- spectra, in the case of taking into account the in–medium effects on secondary nucleons. Therefore, we are confident that our approach is realistic enough to describe the K^+ production through the $\pi N \to K^+Y$ reactions.

Now, let us discuss the results of our calculations for kaon production in pBe and pC interactions in the framework of model outlined above.

3 Results and discussion

Figure 4 shows a comparison of the calculated invariant cross sections for the production of K^+ mesons with momentum of 1.28 GeV/c at the laboratory angle of 10.5^0 from primary $pN \to K^+YN$ and secondary $\pi N \to K^+Y$ channels with the experimental data [11] for $p + Be^9 \to K^+ + X$ reaction at the various bombarding energies. One can see that:

1) our model for primary and secondary kaon production processes, based on nucleon spectral function, fails completely to reproduce the experimental data at subthreshold beam energies (at energies $\leq 2.1\ GeV$ for the kinematical conditions of the experiment [11]) without allowance for the influence of the corresponding effective potentials on the one–step (1), (2) and two–step (20)–(23) production processes;
2) our calculations for the one–step reaction channels (1), (2) with the set of parameters $V_0 = 40\ MeV$, $U^N_{eff} = -34\ MeV$, $U^\Lambda_{eff} = -30\ MeV$, $U^\Sigma_{eff} = -26\ MeV$ (see, (6)) reproduce quite well the experimental data [11] in the energy region far below the lowest threshold, but overestimate the data by a factor of 2 at higher bombarding energies, what indicates that there is no need for employing the medium effects considered by us at these energies;

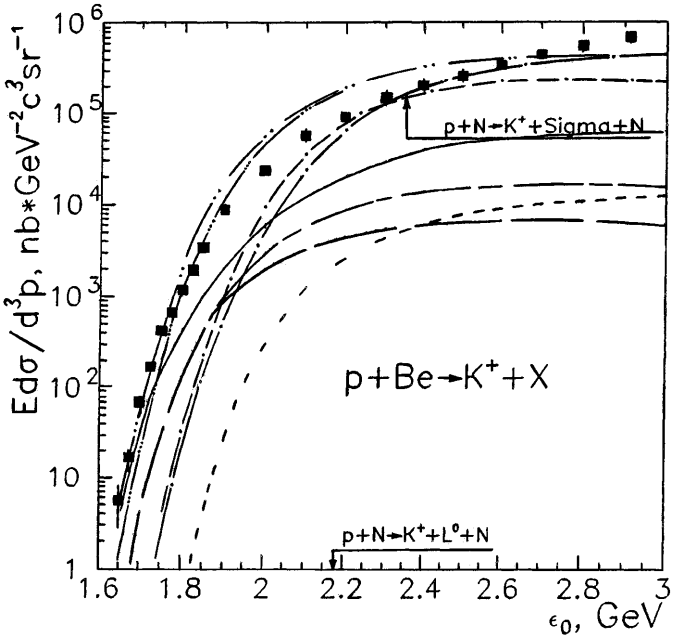

Fig. 4. Lorentz invariant cross sections for the production of K^+ mesons with momentum of 1.28 GeV/c at the lab angle of 10.5^0 in $p+Be^9$ reactions as functions of the laboratory energy of the proton. The experimental data (full squares) are from [11]. The curves are our calculation. The dashed lines with one, two and three dots are calculations for primary production processes (1), (2) with the total nucleon spectral function at $V_0 = 0$, $U^N_{eff} = 0$, $U^\Lambda_{eff} = 0$, $U^\Sigma_{eff} = 0$; $V_0 = 40\ MeV$, $U^N_{eff} = -34\ MeV$, $U^\Lambda_{eff} = -30\ MeV$, $U^\Sigma_{eff} = -26\ MeV$ and $V_0 = 40\ MeV$, $U^N_{eff} = -34\ MeV$, $U^\Lambda_{eff} = -20\ MeV$, $U^\Sigma_{eff} = -26\ MeV$, respectively. The two–dash–dotted line represents our calculations for primary production process (2) with the total nucleon spectral function at $V_0 = 40\ MeV$, $U^N_{eff} = -34\ MeV$, $U^\Sigma_{eff} = -26\ MeV$. The solid line denotes the same as the dashed line with two dots, but it is supposed that the total nucleon spectral function is replaced by its correlated part. The short– and long–dashed lines are calculations for the secondary production process (22) at $V_0 = 0$, $U^N_{eff} = 0$, $U^\Lambda_{eff} = 0$ and $V_0 = 40\ MeV$, $U^N_{eff} = -34\ MeV$, $U^\Lambda_{eff} = -30\ MeV$, respectively. The line with alternating short and long dashes represents calculations for the secondary production processes (22), (23) at $V_0 = 40\ MeV$, $U^N_{eff} = -34\ MeV$, $U^\Lambda_{eff} = -30\ MeV$, $U^\Sigma_{eff} = -26\ MeV$. The arrows indicate the thresholds for the reactions $pN \to K^+\Lambda N$ and $pN \to K^+\Sigma N$ occuring on a free nucleon

3) the results of our calculations of the kaon yield from the two–step reaction channels (20)–(23) with the same set of parameters for the effective potentials V_0, U^N_{eff}, U^Λ_{eff}, U^Σ_{eff} as that used above in the calculating the K^+ yield from the primary reaction channels (1), (2) underestimate essentially the data [11] both at subthreshold and above threshold incident energies, what means the dominance of the one–step K^+ production mechanism for the considered "hard" kaon production at all beam energies of interest;
4) the contributions to the K^+ production from the primary reaction channels (1) and (2) with Λ and Σ particles in the final states are comparable at bombarding energies $\epsilon_0 \geq 2.2\ GeV$, whereas at lower incident energies the primary production process (1) is essentially more important than (2);
5) the primary proton–nucleon production process (1) misses the experimental data in the far subthreshold region when the effective potential U^Λ_{eff} that is seen inside the nucleus by a slow Λ particle increases from the value of $U^\Lambda_{eff} = -30\ MeV$, estimated from the study of the binding and decay of hypernuclei, to $U^\Lambda_{eff} = -20\ MeV$, what implies the strong sensitivity of "hard" kaon yield at "low" beam energies to the lambda potential in the nuclear matter;
6) the kaon yield from the one–step K^+ production mechanism is entirely governed by the correlated part $P_1(\mathbf{p}_t, E)$ of the nucleon spectral function only in the vicinity of the absolute reaction threshold (at bombarding energies of $\epsilon_0 \approx 1.65$–$1.70\ GeV$), what makes difficult to extract the information on the high momentum and high removal energy components within the target nucleus even from the "hard" kaon production experiment [11].

It should be emphasized that the overall calculated kaon spectrum (denoted by the dashed line with two dots in Fig. 4) is not very sensitive to the effective potential U^Σ_{eff} in the subthreshold energy region, since the one–step kaon production process (2) plays a minor role here. Thus, changing this potential from the value of $U^\Sigma_{eff} = -26\ MeV$ used above to the values of $U^\Sigma_{eff} = -10\ MeV$ and $U^\Sigma_{eff} = 20\ MeV$, respectively, employed in [61] in the analysis of the charged pion spectra in the K^- absorption reaction at rest on C^{12} and inferred in [62] from the studying of the (K^-, π^+) reaction on Be^9, as showed our calculations, does not affect practically the overall kaon spectrum at beam energies $\epsilon_0 \leq 2.2\ GeV$ and reduces it approximately by 10% at higher incident energies. Therefore, inclusive subthreshold and near threshold kaon production in pA collisions does not permit to differentiate the scenario with an attractive Σ potential from that with repulsive Σ potential.

The results of our calculations for the double differential cross sections for the production of "soft" K^+ mesons from primary $pN \to K^+YN$ and secondary $\pi N \to K^+Y$ channels at an angle of 40^0 in the interaction of protons with energies of 1.2, 1.5 and 2.5 GeV with C^{12} nuclei and the experimental data [8] are considered in Figs. 5–7. It is seen that:

1) our model calculations for proton and pion induced reaction channels underpredict significantly the data at 1.2 and 1.5 GeV incident energies without taking into account the medium effects on the hadrons produced in these channels, what is consistent with our previous findings of Fig. 4;
2) the inclusion of the in–medium effects under consideration leads to the substantial enhancement of the K^+ cross sections both from primary and secondary kaon

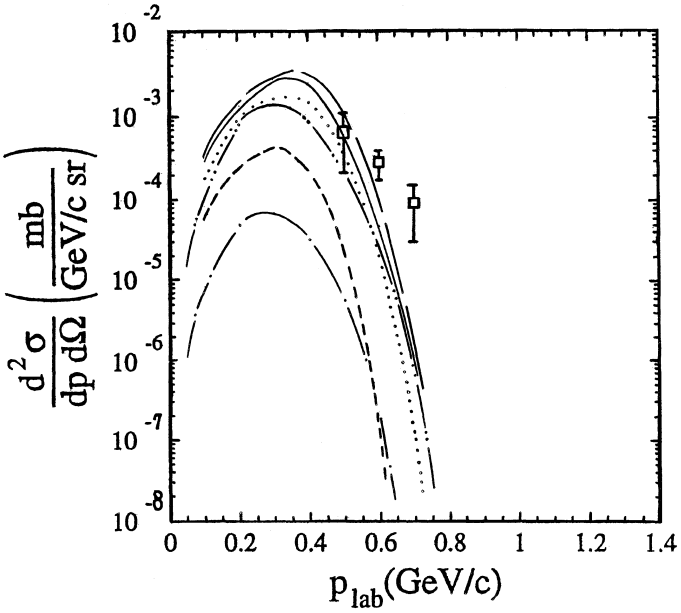

Fig. 5. Double differential cross sections for the production of K^+ mesons at an angle of 40^0 in the interaction of 1.2 GeV protons with the C^{12} nuclei as functions of kaon momentum. The experimental data (open squares) are from [8]. The curves are our calculation. The dashed lines with one and two dots are calculations for primary production process (1) with the total nucleon spectral function at $V_0 = 0$, $U^N_{eff} = 0$, $U^\Lambda_{eff} = 0$ and $V_0 = 40\ MeV$, $U^N_{eff} = -34\ MeV$, $U^\Lambda_{eff} = -30\ MeV$, respectively. The short–, long–dashed and dotted lines are calculations for the secondary production process (22) at $V_0 = 0$, $U^N_{eff} = 0$, $U^\Lambda_{eff} = 0$; $V_0 = 40\ MeV$, $U^N_{eff} = -34\ MeV$, $U^\Lambda_{eff} = -30\ MeV$ and $V_0 = 40\ MeV$, $U^N_{eff} = -34\ MeV$, $U^\Lambda_{eff} = 0$, respectively. The thin solid line is the sum of the dashed line with two dots and dotted line

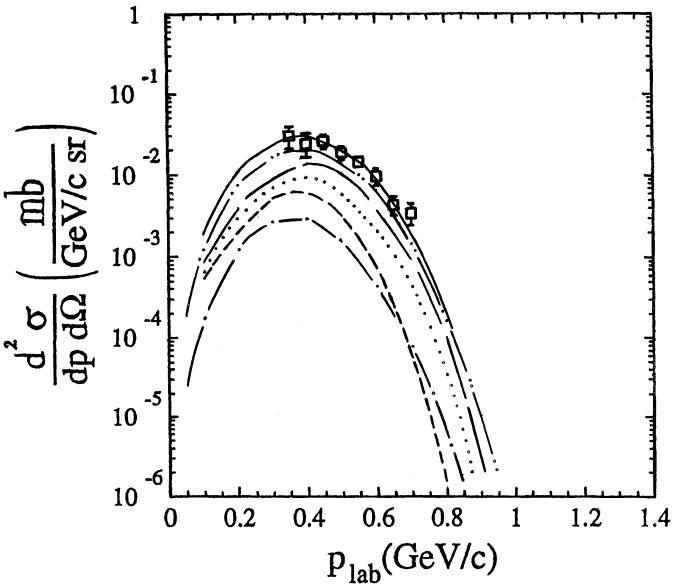

Fig. 6. Double differential cross sections for the production of K^+ mesons at an angle of 40^0 in the interaction of 1.5 GeV protons with the C^{12} nuclei as functions of kaon momentum. The dashed lines with one and two dots are calculations for primary production processes (1), (2) with the total nucleon spectral function at $V_0 = 0$, $U^N_{eff} = 0$, $U^\Lambda_{eff} = 0$, $U^\Sigma_{eff} = 0$ and $V_0 = 40\ MeV$, $U^N_{eff} = -34\ MeV$, $U^\Lambda_{eff} = -30\ MeV$, $U^\Sigma_{eff} = -26\ MeV$, respectively. The rest of the notation is identical to that in Figure 5

production processes at 1.2 and 1.5 GeV beam energies as well as to the similar magnitude[4] for these K^+ creation processes at indicated bombarding energies;

3) the "soft" kaon yield from the secondary reaction channel (22) with Λ particle in the final state at 1.2 and 1.5 GeV beam energies is not very sensitive to the effective potential U^Λ_{eff} that is seen inside the nucleus by a lambda when this potential increases from $U^\Lambda_{eff} = -30\ MeV$ to $U^\Lambda_{eff} = 0$ and moreover, the difference between the calculations with allowance for the influence of this potential on the production process (22) and without it increases with decreasing incident energy;
4) the one–step K^+ production mechanism clearly dominates at 2.5 GeV proton beam energy both with and without including the influence of the mean fields on the one–step production processes (1), (2);
5) the high momentum tail[5] ($p_{lab} \geq 0.9\ GeV/c$) of the kaon spectrum measured in [8] at 2.5 GeV incident energy is much better reproduced by our first chance collision model when including the same influence of the mean fields on the one–step production processes (1), (2) as that employed above (see Fig. 4) in the analysis of the energy dependence of the "hard" kaon production taken in [11], whereas its low momentum tail ($p_{lab} \leq 0.6\ GeV/c$) is reasonably well described by the model both with and without including this influence;
6) our overall calculations (the sum of results obtained both for the one–step (1), (2) and two–step (20)–(23) reaction channels, thin solid lines in Figs. 5–7) reproduce reasonably the experimental data only if we include the effect of the respective effective potentials on the one–step kaon production processes (1), (2) and on pion production reactions (20), (21).

The results presented in Figs. 5, 6 indicate that the better description of the data is achieved when we discard the effective potential U^Λ_{eff} seen inside the nucleus by lambdas from the secondary production process (22). This is realistic enough, since the spatial creation points of hy-

[4] It should be mentioned that the first chance collision models [8, 10], based on nucleon spectral function as well as on discarding any self–energies for the produced hadrons, predict a minor role for the direct K^+ production processes (1), (2) compared to that for the secondary K^+ reaction channels (22), (23) in subthreshold kaon production in pC interactions at these bombarding energies.

[5] It should be noticed that for kinematical conditions of the experiment [8] the kaons emitted with the laboratory momenta $p_{lab} \geq 0.9\ GeV/c$ are subthreshold kaons.

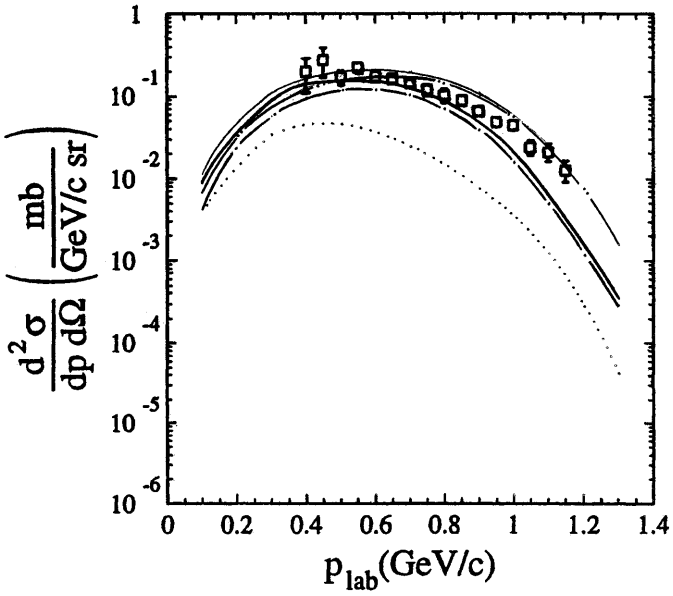

Fig. 7. Double differential cross sections for the production of K^+ mesons at an angle of 40^0 in the interaction of 2.5 GeV protons with the C^{12} nuclei as functions of kaon momentum. The dotted line is calculation for the secondary production processes (22) and (23) at $V_0 = 40\ MeV$, $U^N_{eff} = -34\ MeV$, $U^\Lambda_{eff} = 0$, $U^\Sigma_{eff} = 0$. The dashed lines with one and two dots, the thin solid line denote the same as in Figure 6. The thick solid line is the sum of the dash–dotted and dotted lines

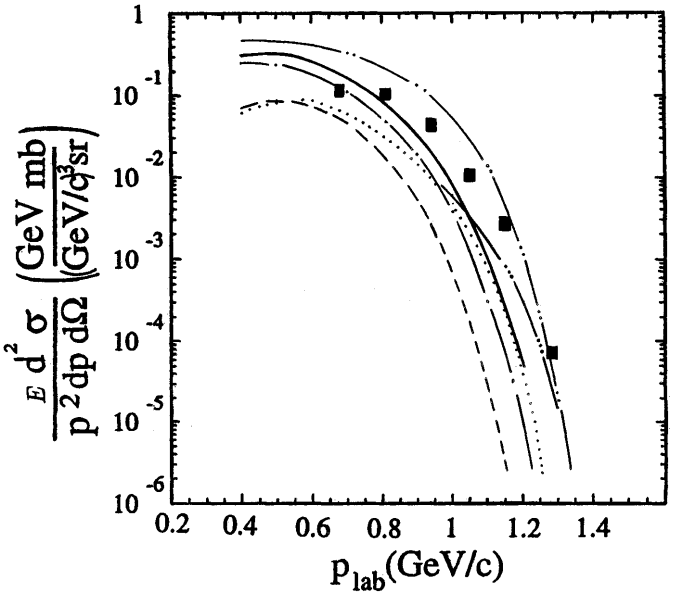

Fig. 8. Lorentz invariant inclusive cross sections for the production of K^+ mesons at an angle of 10.5^0 in the interaction of 1.7 GeV protons with the Be^9 nuclei as functions of kaon momentum. The experimental data (full squares) are from [12]. The curves are our calculation. The dashed lines with one and two dots are calculations for primary production processes (1), (2) with the total nucleon spectral function at $V_0 = 0$, $U^N_{eff} = 0$, $U^\Lambda_{eff} = 0$, $U^\Sigma_{eff} = 0$ and $V_0 = 40\ MeV$, $U^N_{eff} = -34\ MeV$, $U^\Lambda_{eff} = -30\ MeV$, $U^\Sigma_{eff} = -26\ MeV$, respectively. The dashed line with three dots denotes the same as the dashed line with two dots, but it is supposed that the total nucleon spectral function is replaced by its correlated part. The short–dashed and dotted lines are calculations for the secondary production processes (22), (23) at $V_0 = 0$, $U^N_{eff} = 0$, $U^\Lambda_{eff} = 0$, $U^\Sigma_{eff} = 0$ and $V_0 = 40\ MeV$, $U^N_{eff} = -34\ MeV$, $U^\Lambda_{eff} = 0$, $U^\Sigma_{eff} = 0$, respectively. The thick solid line is the sum of the dash–dotted and dotted lines

perons due to secondary πN collisions are shifted to the periphery of the target nucleus (where the nuclear density is smaller than that inside of it) in comparison to those from primary pN events [34]. Therefore, we will neglect the self–energies for hyperons from pion induced reactions (22), (23) in the further calculations. It is evident that in this case the kaon yield from the two–step reaction channels (20)–(23), calculated in the kinematical conditions of the experiment [11] (see Fig. 4), will be less (by a factor of 5 as showed our calculations) than that obtained with the set of potential parameters (6) (the line with alternating short and long dashes in Fig. 4) at subthreshold bombarding energies. This fact is also in line with the conclusion deduced above that the direct K^+ production mechanism dominates in the subthreshold "hard" kaon production in pBe^9 interactions [11].

It should be pointed out that the two–pion production reactions (21) have been taken into account in the above calculations only at 2.5 GeV incident laboratory kinetic energy, where their contribution to the inelastic cross sections of free pN interaction is about 40%. It is worth also mentioning that the present model can simultaneously reproduce the π^+ spectra measured in the same experiment [8] (see Fig. 3).

Figure 8 presents a comparison of the results of our calculations for the Lorentz invariant inclusive cross sections for the production of K^+ mesons at the laboratory angle of 10.5^0 from proton and pion induced reaction channels with the experimental data [12] for $p + Be^9 \to K^+ + X$ reaction at 1.7 GeV beam energy. It can be seen that:

1) the model calculations for primary and secondary kaon production processes underestimate substantially the subthreshold data points[6], as in the above cases (cf. Figs. 4–7), without including the in–medium effects considered by us;
2) the high momentum part of the measured kaon spectrum is fairly well reproduced by the calculations for the one–step production processes (1), (2) with allowance for the same influence of the nuclear mean fields on these processes as that adopted above in the analysis of another experimental data [8, 11] on subthreshold kaon production in pBe and pC collisions (see Figs. 4–7), whereas its low momentum part is overestimated by calculations by a factor of about 2–3;
3) our calculations of the kaon yield from the two–step production processes (20)–(23) with the same set of

[6] It should be noted that for kinematical conditions of the experiment [12] the data points which correspond to the laboratory kaon momenta $p_{lab} \geq 0.8\ GeV/c$ are the subthreshold data points.

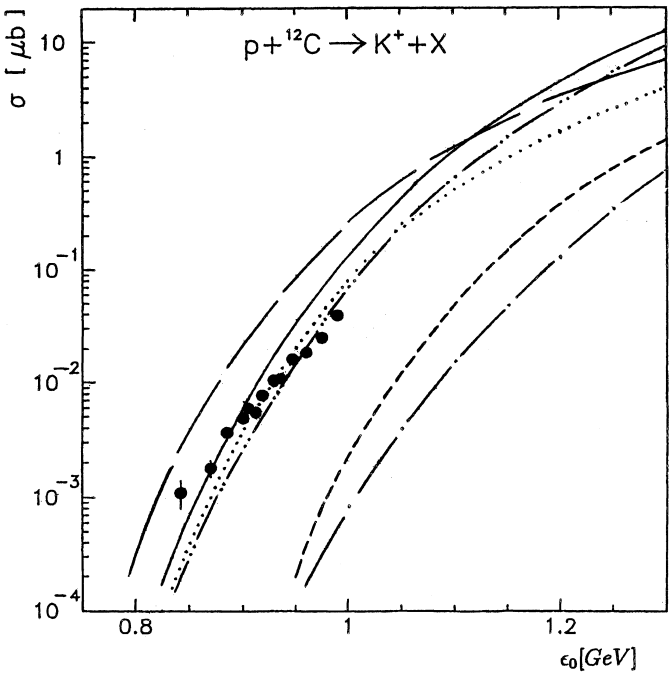

Fig. 9. The total cross sections for K^+ production in $p + C^{12}$ reactions as functions of the laboratory energy of the proton. The experimental data (full dots) are from [1]. The curves are calculation. The dashed lines with one and two dots are calculations for primary production processes (1), (2) with the total nucleon spectral function at $V_0 = 0$, $U^N_{eff} = 0$, $U^\Lambda_{eff} = 0$, $U^\Sigma_{eff} = 0$ and $V_0 = 40\ MeV$, $U^N_{eff} = -34\ MeV$, $U^\Lambda_{eff} = -30\ MeV$, $U^\Sigma_{eff} = -26\ MeV$, respectively. The short–, long–dashed and dotted lines are calculations for the secondary production process (22) with Λ particle in the final state at $V_0 = 0$, $U^N_{eff} = 0$, $U^\Lambda_{eff} = 0$; $V_0 = 40\ MeV$, $U^N_{eff} = -34\ MeV$, $U^\Lambda_{eff} = -30\ MeV$ and $V_0 = 40\ MeV$, $U^N_{eff} = -34\ MeV$, $U^\Lambda_{eff} = 0$, respectively. The thin solid line is the sum of the dashed line with two dots and dotted line

parameters for the effective potentials V_0, U^N_{eff}, U^Λ_{eff} and U^Σ_{eff} as that employed above (see Figs. 5–7) in the analysis of the corresponding K^+ yield from pC interactions underpredict significantly the subthreshold data points, what indicates the dominance of the one–step K^+ production mechanism at the laboratory kaon momenta $p_{lab} > 0.8\ GeV/c$;

4) the high momentum tail of the kaon spectrum from direct K^+ production mechanism is almost completely determined by the correlated part $P_1(\mathbf{p}_t, E)$ of the nucleon spectral function only in a very limited range of kaon momenta ($p_{lab} \approx 1.25$–$1.35\ GeV/c$), what makes difficult to extract this part from the experimental data [12].

In Fig. 9 we compare the results of our calculations for the total cross sections for K^+ production in pC^{12} collisions from primary $pN \to K^+YN$ and secondary $\pi N \to K^+\Lambda$ channels with the experimental data [1]. It is clearly seen that:

1) the calculations for primary and secondary kaon production channels miss essentially the data in line with our findings inferred above from the analysis of the data on differential kaon production cross sections when no self–energy effects have been employed and moreover, the primary pN and secondary πN channels are of the same order of magnitude in this case;
2) approximately an equal magnitude[7] for these channels is gained at beam energies below about 1.1 GeV when the same influence of the nuclear mean fields on them (the set of potential parameters (6) for the direct K^+ production processes (1), (2) and the set of parameters: $U^N_{eff} = -34\ MeV$, $U^\Lambda_{eff} = 0$ for the two-step reaction channels (20)–(22)) as that allowed us to describe the existing experimental data [8, 11, 12] on the differential kaon production cross sections (cf. Figs. 4–8) has been included;
3) our full calculations (the sum of results obtained both for the one–step (1), (2) and two–step (20)–(22) reaction channels, thin solid line in Fig. 9), which adopted the effect of the respective effective potentials on these channels, reproduce reasonably well the measured [1] total K^+ production cross sections[8] at proton energies below about 900 MeV, but overestimate slightly the data at higher bombarding energies.

Clearly the enhanced K^+ production via first–chance pN collisions (1), (2) (dashed line with two dots in Fig. 9) is due to the in–medium reduction of the masses of final nucleon and hyperon that leads to the lowered effective kaon creation thresholds in line with (18). Whereas the increased cross sections for K^+ production through secondary process $\pi N \to K^+\Lambda$ are caused by both the in–medium Λ mass reduction due to an attractive effective lambda–nucleus potential U^Λ_{eff} and an enhanced fast pion production (see Figs. 2, 3) from primary proton induced reaction channels (20), (21) due to an effective nucleon–

[7] It should be emphasized that this finding is in disagreement with the conclusions of the authors of earlier studies [3–5] of the measured [1] total cross sections for K^+ production from pA collisions in the framework of the simple folding models who claim the dominance of the secondary πN channel for K^+ production in proton–nucleus reactions at subthreshold energies. This result disagrees also with the recent studies [9, 10] of the data [1] on total K^+ production cross section from pC interactions within the spectral function approach without including any self–energy effects for the hadrons created in direct processes (1) (2), since it has been claimed in [9, 10] that the two–step kaon production mechanism with an intermediate pion dominates in subthreshold regime as in the folding models [3–5].

[8] It is interesting to note that we are able to reproduce reasonably these cross sections also within the simple folding model (cf. [3–5]) for the two–step K^+ production mechanism ($pN_1 \to \pi NN$, $\pi N_2 \to K^+\Lambda$) which is obtained from the present model by replacing the total nucleon spectral function on the shell–model momentum distribution (30) [10], assuming the struck target nucleon to be on–mass shell as well as employing only the repulsive optical potential of about $V_0 \approx 50\ MeV$ in the entrance channel in line with [3, 5, 9].

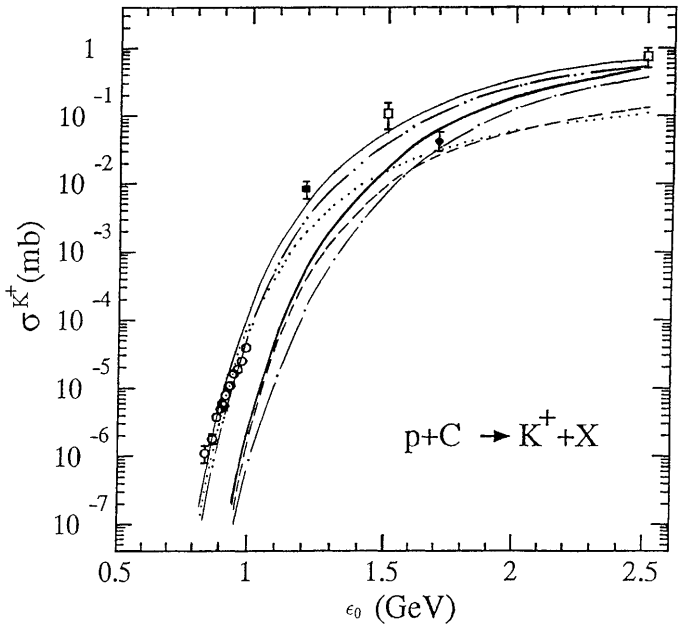

Fig. 10. The total cross sections for K^+ production in $p+C^{12}$ reactions as functions of the laboratory energy of the proton. The experimental data are from [1, 8, 63, 64]. The curves are calculation. The short–dashed and dotted lines are calculations for the two–step production processes (20)–(23) at $V_0 = 0$, $U^N_{eff} = 0$, $U^\Lambda_{eff} = 0$, $U^\Sigma_{eff} = 0$ and $V_0 = 40\ MeV$, $U^N_{eff} = -34\ MeV$, $U^\Lambda_{eff} = 0$, $U^\Sigma_{eff} = 0$, respectively. The thick solid line is the sum of the dot–dashed and short–dashed lines. The rest of the notation is identical to that in Figure 9

nucleus potential U^N_{eff} (long–dashed line) as well as by only enhanced fast pion production alone (dotted line).

Finally, Fig. 10 shows the same comparison as that presented in Fig. 9, but includes also data points at proton energies of 1.2, 1.5, 1.7 and 2.5 GeV. The data point at 1.2 GeV was taken from the recently published paper [63] in which it has been inferred from the measured double differential cross sections for "soft" kaon production at the laboratory angles of 40^0 [8] and 90^0 [63] for this bombarding energy. The data points at 1.5 and 2.5 GeV were taken from [8], where the ones have been deduced from the measured K^+ double differential cross sections at these incident energies (see Figs. 6, 7). And the data point at 1.7 GeV was taken from [64], where it has been extracted from the inclusive invariant cross sections for kaon production in pBe^9 interactions, given in Fig. 8, assuming an $A^{2/3}$ scaling to make an extrapolation from Be^9 to C^{12} target nuclei. It is nicely seen that our overall model calculations (the sum of results obtained both for primary and secondary kaon production processes, thin solid line in Fig. 10) with including the same mean–field effects as those, allowed us to describe above the data both on differential [8, 11, 12] and total [1] kaon production cross sections, reproduce fairly good also the measured [8, 63] total K^+ production cross sections at proton energies of 1.2, 1.5, 2.5 GeV and overestimate the data point [64] at 1.7 GeV by a factor of about 3[9]. Whereas the similar calculations with no mean–field effects (thick solid line in Fig. 10) describe reasonably both this data point and that at 2.5 GeV, but fail completely to reproduce the data at lower incident energies, what counts in favour of the former model calculations. It is also seen that at beam energies below about 1.5 GeV the contributions from the two–step and one–step kaon production processes are comparable in both calculations.

Taking into account the considered above, one may conclude that the relative strength of the proton and pion induced reaction channels in light target nuclei in the subthreshold energy regime is mainly governed by the kinematics of experiment on inclusive kaon production in pA interactions. Our results demonstrate also that further measurements of the total (and differential) cross sections for K^+ production on light nuclei in the proton–energy range 1.0–1.7 GeV are extremely needed nowadays to reliably test the spectral function approach presented in this study as well as to deeply elucidate the underlying mechanism of subthreshold kaon production and the role played by nucleon–nucleon correlations in this phenomenon. Such measurements might be made at, for example, the CELSIUS storage ring of the Uppsala The Svedberg Laboratory and the Cooler Synchrotron COSY–Jülich.

4 Summary

In this study we have calculated the total and differential cross sections for K^+ production from pBe^9 and pC^{12} reactions in the near threshold and subthreshold energy regimes by considering incoherent primary proton–nucleon and secondary pion–nucleon production processes in the framework of an appropriate folding model, which takes properly into account the struck target nucleon momentum and removal energy distribution, novel elementary cross sections for proton–nucleon reaction channel close to threshold as well as nuclear mean–field potential effects on the one–step and two–step kaon production processes. The detailed comparison of the results of our calculations with the existing experimental data [1, 8, 11, 12, 63] was made. It was shown that these effects are of importance in consistent explaining both the considered experimental data on kaon production and the measured [8, 59, 60] at forward angles charged pion spectra from pC^{12} interactions at beam energies between 1.05 and 2.1 GeV. It was also found that, contrary to previous studies carried out in the literature, the pion–nucleon production channels do not necessarily dominate in pA collisions at subthreshold energies and the relative weight of the proton and pion induced reaction channels in light target nuclei in the subthreshold energy regime is governed by the kinematics of experiment under consideration, namely: the one–step K^+ production mechanism clearly dominates in the subthreshold "hard" kaon production in pBe^9 [11, 12]

[9] Compare to the analogous difference in low momentum region between the measured and calculated kaon production cross sections presented in Fig. 8.

and pC^{12} [8] collisions, whereas in the subthreshold "soft" kaon production in pC^{12} reactions [1, 8, 63] the contributions from the direct and two–step kaon production processes are comparable. Our present results indicate that the kaon yield from the one–step K^+ production mechanism is almost completely determined by the correlated part of the nucleon spectral function only in a very limited range of kaon momenta (for kaon spectra) or bombarding energies (for energy dependence), what makes difficult to extract it from the data under consideration. Therefore, further measurements of the differential cross sections for subthreshold "hard" K^+ production on light nuclei are needed both to reliably test the spectral function approach presented in this work and to deeply elucidate the underlying mechanism of subthreshold kaon production and the role played by nucleon–nucleon correlations in this phenomenon.

I am very grateful to Yu.T.Kiselev and V.A.Sheinkman for their information on experimental results from the ITEP synchrotron on near threshold and subthreshold kaon production in proton–nucleus collisions as well as for valuable discussions throughout this study. I am also thankful to L.A. Kondratyuk for interest in the work.

References

1. Koptev, V.P., Mikirtyhyants, S.M., Nesterov, M.M., Tarasov, N.A., Shcherbakov, G.V., Abrosimov, N.K., Volchenkov, V.A, Gridnev, A.B., Yeliseyev, V.A., Ivanov, E.M., Kruglov, S.P., Malov, Yu.A., Ryabov, G.A.: *ZhETF.* **94**, 1 (1988)
2. Shor, A., Perez-Mendez, V., Ganezer, K.: *Nucl. Phys.* **A514**, 717 (1990)
3. Cassing, W., Batko, G., Mosel, U., Niita, K., Schult, O., Wolf, Gy.: *Phys. Lett.* **238B**, 25 (1990)
4. Sibirtsev, A.A., Büscher, M.: *Z. Phys.* **A347**, 191 (1994)
5. Cassing, W., Demski, T., Jarczyk, L., Kamys, B., Rudy, Z., Schult, O.W.B., Strzalkowski, A.: *Z. Phys.* **A349**, 77 (1994)
6. Sibirtsev, A.: *Phys. Lett.* **359B**, 29 (1995)
7. Müller, H., Sistemich, K.: *Z. Phys.* **A344**, 197 (1992)
8. Debowski, M., Barth, R., Boivin, M., Le Bornec, Y., Cieslak, M., Comets, M.P., Courtat, P., Gacougnolle, R., Grosse, E., Kirchner, T., Martin, J.M., Miskowiec, D., Müntz, C., Schwab, E., Senger, P., Sturm, C., Tatischeff, B., Wagner, A., Walus, W., Willis, N., Wurzinger, R., Yonnet, J., Zghiche, A.: *Z. Phys.* **A356**, 313 (1996)
9. Sibirtsev, A., Cassing, W., Mosel, U.: *Z. Phys.* **A358**, 357 (1997)
10. Efremov, S.V., Paryev, E.Ya.: *Eur. Phys. J.* **A1**, 99 (1998)
11. Akindinov, A.V., Chumakov, M.M., Kiselev, Yu.T., Martemyanov, A.N., Mikhailov, K.R., Pozdnyakov, S.A., Sheinkman, V.A., Terekhov, Yu.V.: *APH N.S., Heavy Ion Physics* **4**, 325 (1996)
12. Kiselev, Yu.T., Firozabadi, M.M., Ushakov, V.I.:*Preprint ITEP* **56–96**, Moscow (1996)
13. Oelert, W.: *Nucl. Phys.* **A639**, 13c (1998); Balewski, J.T., Budzanovski, A., Dombrowski, H., Eyrich, W., Goodman, C., Grzonka, D., Haidenbauer, J., Hanhart, C., Hauffe, J., Jarczyk, L., Jochmann, M., Khoukaz, A., Kilian, K., Kohler, M., Kozela, A., Lister, T., Metzger, A., Moskal, P., Oelert, W., Quentmeier, C., Santo, R., Schepers, G., Seddik, U., Sefzick, T., Smyrski, J., Sokolowski, M., Stinzing, F., Strzalkowski, A., Thomas, C., Wirth, S., Wolke, M., Woodward, R., Wustner, P., Wyrwa, D.: *LANL Preprint* **Nucl–ex/9803003** (1998); Eyrich, W.: *Strangeness Production in Proton–Proton Reactions at COSY–TOF.* In "Proc. of the Seventh Int. Symp. on Meson–Nucleon Physics and the Structure of the Nucleon", p.373. Vancouver, British Columbia, Canada, July 28–August 1, (1997)
14. Cassing, W., Bratkovskaya, E.L., Mosel, U., Teis, S., Sibirtsev, A.: *Nucl. Phys.* **A614**, 415 (1997)
15. Bratkovskaya, E.L., Cassing, W., Mosel, U.: *Nucl. Phys.* **A622**, 593 (1997)
16. Efremov, S.V., Kazarnovsky, M.V., Paryev, E.Ya.: *Z. Phys.* **A344**, 181 (1992)
17. Kaplan, D.B., Nelson, A.E.: *Phys. Lett.* **175B**, 57 (1986); Nelson, A.E., Kaplan, D.B.: *Phys. Lett.* **192B**, 193 (1987)
18. Fuchs, C., Wang, Z., Sehn, L., Faessler, A., Uma Maheswari, V.S., Kosov, D.S.: *Phys. Rev.* **C56**, R606 (1997)
19. Li, G.Q., Ko, C.M., Li, Bao–An.: *Phys. Rev Lett.* **74**, 235 (1995)
20. Li, G.Q., Ko, C.M.: *Nucl.Phys.* **A594**, 460 (1995)
21. Li, Bao–An, Ko, C.M.: *Phys. Rev.* **C54**, 3283 (1996)
22. Waas, T., Kaiser, N., Weise, W.: *Phys. Lett.* **379B**, 34 (1996)
23. Schaffner, J., Mishustin, I.N.: *Phys. Rev.* **C53**, 1416 (1996)
24. Brown, G.E., Rho, M.: *Nucl.Phys.* **A596**, 503 (1996)
25. Waas, T., Rho, M., Weise, W.: *Nucl.Phys.* **A617**, 449 (1997)
26. Brown, G.E., Ko, C.M., Li, G.Q.: *LANL Preprint* **Nucl–th/9608039** (1996)
27. Cassing, W., Lang, A., Teis, S., Weber, K.: *Nucl. Phys.* **A545**, 123c (1992)
28. Cahay, M., Cugnon, J., Vandermeulen, J.: *Nucl. Phys.* **A411**, 524 (1983)
29. Teis, S., Cassing, W., Effenberger, M., Hombach, A., Mosel, U., Wolf, Gy.: *Z. Phys.* **A356**, 421 (1997)
30. Goncalves, M., de Pina, S., Lima, D.A., Milomen, W., Medeiros, E.L., Duarte, S.B.: *Phys. Lett.* **406B**, 1 (1997)
31. Teis, S., Cassing, W., Maruyama, T., Mosel, U.: *Phys. Rev.* **C50**, 388 (1994)
32. Ehehalt, W., Cassing, W.: *Nucl.Phys.* **A602**, 449 (1996)
33. Lee, C.H., Kuo, T.T.S., Li, G.Q., Brown, G.E.: *Phys. Lett.* **412B**, 235 (1997)
34. Rudy, Z., Cassing, W., Demski, T., Jarczyk, L., Kamys, B., Kulessa, P., Schult, O.W.B., Strzalkowski, A.: *Z. Phys.* **A351**, 217 (1995)
35. Yamamoto, Y., Bando, H.: *Phys. Lett.* **214B**, 173 (1988)
36. Hjorth–Jensen, M., Polls, A., Ramos, A., Muther, H.: *Nucl.Phys.* **A605**, 458 (1996)
37. Li, G.Q., Ko, C.M.: *Phys. Rev.* **C54**, 1897 (1996)
38. Fang, X.S., Ko, C.M., Li, G.Q., Zheng, Y.M.: *Nucl. Phys.* **A575**, 766 (1994)
39. Fang, X.S., Ko, C.M., Li, G.Q., Zheng, Y.M.: *Phys.Rev.* **C49**, R608 (1994)
40. Dalitz, R.H., Gal, A.: *Phys. Lett.* **64B**, 154 (1976)
41. Dover, C.B., Walker, G.E.: *Phys. Rep.* **89**, 1 (1982)
42. Li, G.Q., Ko, C.M.: *Phys. Lett.* **349B**, 405 (1995)
43. Ciofi degli Atti, C., Simula, S.: *Phys. Lett.* **325B**, 276 (1994)

44. Ciofi degli Atti, C., Pace, E., Salme, G.: *Phys. Rev.* **C43**, 1155 (1991)
45. Fickinger, W.J.: *Phys. Rev.* **125**, 2082 (1962)
46. Ciofi degli Atti, C., Liuti, S.: *Phys. Lett.* **225B**, 215 (1989)
47. Ciofi degli Atti, C., Liuti, S., Simula, S.: *Phys. Rev.* **C41**, R2474 (1990)
48. Ciofi degli Atti, C., Simula, S., Frankfurt, L.L., Strikman, M.I.: *Phys. Rev.* **C44**, R7 (1991)
49. Benhar, O., Fabrocini, A., Fantoni, S., Sick, I.: *Nucl. Phys.* **A579**, 493 (1994)
50. Ciofi degli Atti, C., Simula, S.: *Phys. Rev.* **C53**, 1689 (1996)
51. Weinstein, L.B., Warren, G.A.: *Phys. Rev.* **C50**, 350 (1994)
52. Ciofi degli Atti, C.: *Nuovo Cimento* **76A**, 330 (1983)
53. Jacob, G., Maris, Th.: *Rev. Mod. Phys.* **38**, 121 (1966); **45**, 6 (1973)
54. Tyren, H.: *Nucl.Phys.* **79**, 321 (1966)
55. Bystricky, J., La France, P., Lehar, F., Perrot, F., Siemiarczuk, T., Winternitz, P.: *J.de Physique.* **48**, 1901 (1987)
56. Cugnon, J., Lombard, R.M.: *Nucl.Phys.* **A422**, 635 (1984)
57. Tsushima, K., Huang, S.W., Faessler, A.: *Phys. Lett.* **337B**, 245 (1994)
58. Jones, J.J., Bowen, T., Dawes, W.R., DeLise, D.A., Jenkins, E.W., Kalbach, R.M., Malamud, E.I., Nield, K.J., Petersen, D.V.: *Phys. Rev. Lett.* **26**, 860 (1971)
59. Moeller, E., Anderson, L., Bruckner, W., Nagamiya, S., Nissen–Meyer, S., Schroeder, L., Shapiro, G., Steiner, H.: *Phys. Rev.* **C28**, 1246 (1983)
60. Papp, J., Jaros, J., Schroeder, L., Staples, J., Steiner, H., Wagner, A., Wiss, J.: *Phys. Rev. Lett.* **34**, 601 (1975); *Phys. Rev. Lett.* **34**, 991 (1975)
61. Ohnishi, A., Nara, Y., Koch, V.: *Phys. Rev.* **C56**, 2767 (1997)
62. Dabrowski, J., Rozynek, J.: *Acta Phys. Pol.* **B29**, 2147 (1998)
63. Badala, A., Barbera, R., Bassi, M., Bonasera, A., Gulino, M., Librizzi, F., Mascali, A., Palmeri, A., Pappalardo, G.S., Riggi, F., Russo, A.C., Russo, G., Turrisi, R., Dunin, V., Ekstrom, C., Ericsson, G., Hoistad, B., Johansson, J., Johansson, T., Westerberg, L., Zlomaczhuk, J., Sibirtsev, A.: *Phys. Rev. Lett.* **80**, 4863 (1998)
64. Kiselev, Yu.T., Sheinkman, V.A.: Private communication